Experimental and Theoretical Investigation of Structures, Stoichiometric Diversity, and Bench Stability of Cocrystals with a Volatile Halogen Bond Donor

Lisac, Katarina; Nemec, Vinko; Topić, Filip; Arhangelskis, Mihails; Hindle, Poppy; Tran, Ricky; Huskić, Igor; Morris, Andrew J.; Friščić, Tomislav; Cinčić, Dominik

DOI:
10.1021/acs.cgd.7b01808

Experimental and theoretical investigation of structures, stoichiometric diversity and bench stability of cocrystals with a volatile halogen bond donor

Katarina Lisac,[a] *Vinko Nemec,*[a] *Filip Topić,*[b] *Mihails Arhangelskis,*[b] *Poppy Hindle,*[b,c] *Ricky Tran,*[b] *Igor Huskić,*[b] *Andrew J. Morris,*[d] *Tomislav Friščić**[b] *and Dominik Cinčić**[a]

[a] Department of Chemistry, Faculty of Science, University of Zagreb, Horvatovac 102a, HR-10000 Zagreb, Croatia. Fax: 00385-14606341; Tel: +385-1-460-6362; E-mail: dominik@chem.pmf.hr

[b] Department of Chemistry, McGill University, 801 Sherbrooke St. W., Montreal, H3A 0B8, Canada. Fax: +1-514-398-3757; Tel: +1-514-398-3959; E-mail: tomislav.friscic@mcgill.ca

[c] School of Chemistry, Cardiff University, Main Building, Park Place, Cardiff, CF10 3AT, United Kingdom

[d] School of Metallurgy and Materials, University of Birmingham, Edgbaston, Birmingham B15 2TT, United Kingdom

KEYWORDS. Cocrystals, halogen bonding, stability, mechanochemistry, X-ray diffraction

ABSTRACT. We present a combined experimental and theoretical study of the structures and bench stability of halogen-bonded cocrystals involving the volatile halogen bond donor octafluoro-1,4-diiodobutane, with phenazine and acridine as acceptors. Cocrystallization experiments using mechanochemistry and solution crystallization revealed three chemically and structurally distinct cocrystals. Whereas only one cocrystal form has been observed with acridine, cocrystallization with phenazine led to two stoichiometrically different cocrystals, in which phenazine employs either one or two nitrogen atoms per molecule as halogen bond acceptor sites. Cocrystal stability was evaluated experimentally by simultaneous thermogravimetric analysis and differential thermal analysis or differential scanning calorimetry, real-time X-ray powder diffraction monitoring of cocrystals upon storage in open air, and theoretically by using dispersion-corrected periodic density-functional theory (DFT). The use of real-time powder X-ray diffraction enabled the comparison of rates of cocrystal decomposition, and the observed trends in cocrystal stability were reproduced by the ranking of theoretically calculated cocrystal decomposition enthalpies. Whereas all cocrystals eventually lose the volatile halogen bond donor upon storage in open air or by heating, these experimental and theoretical studies show that the cocrystal of acridine is the most stable, in agreement with its more basic properties. The stoichiometric variations of the phenazine cocrystal also exhibit a notable difference in stability, with the cocrystal containing the halogen bond acceptor and donor in a 1:1 stoichiometric ratio being of particularly low stability, decomposing in open air within minutes.

Introduction

Halogen bonds are non-covalent interactions that form between a polarisable halogen atom as a bond donor (typically Br or I) and an electron rich atom as a bond acceptor.[1-3] Similarly to hydrogen bonds, they can be highly directional, and their formation and strength can be modulated by varying the periphery of the molecule to which the halogen atom is bonded. The stability of halogen bonds generally increases with increasing Lewis basicity of the halogen bond acceptor, and increasing Lewis acidity of the donor.[4-6] For example, a recent study comparing the halogen- or hydrogen-bonded cocrystals of succinimide and different *N*-halosuccinimides with an identical set of Lewis bases as hydrogen- or halogen-bond acceptors revealed that in a set of structurally equivalent systems – *i.e.* cocrystals differing only in the nature of the contact atom between cocrystal-forming components, the halogen bonds based on iodine atoms led to supramolecular interactions more stable than hydrogen bonds.[7] Throughout the last decade, halogen bonds have become highly popular for constructing supramolecular architectures, and crystal engineering of molecular solids and functional materials.[8-25]

As a part of our general research program on halogen bonding in the solid state, and in particular aspects of halogen bond donor or acceptor structure that lead to the formation of isostructural materials,[26-28] we now describe the formation and bench stability of halogen-bonded cocrystals of octafluoro-1,4-diiodobutane (**ofib**) halogen bond donor, with acridine (**acr**) and phenazine (**phen**) as acceptors (Figure 1a). Our interest in halogen-bonding properties of **phen** and **acr** is based on their polyaromatic heterocyclic structure[29] which provides a simple entry into halogen bond acceptors that are sterically and electronically different from the much more investigated pyridine- or azole-based acceptors.[30-38] Furthermore, the similarity of molecular structures of **acr** and **phen** offers an excellent opportunity to investigate the effect of exchanging aromatic C-H

and N functionalities on molecular self-assembly in the solid state, and in particular on the formation of isostructural solids.[26,27,39,40] Both **acr** and **phen** are weak bases, with respective pK_a values of 5.58 and 1.23,[28,41,42] and have been used extensively as components of hydrogen-bonded salts and cocrystals.[43,44] However, both molecules have been much less explored as components of halogen-bonded cocrystals. A Cambridge Structural Database (CSD)[45] survey reveals a total of 143 multi-component crystal structures, either salts or cocrystals, containing **acr** and 201 containing **phen**. Among these, hydrogen-bonded or protonated **acr** molecules are found in a total of 77 and 22 structures, respectively. Corresponding numbers for **phen** are 115 and 14, respectively, with the latter value including both singly and doubly protonated **phen**. In contrast, only 15 structures of halogen-bonded cocrystals of either **phen** or **acr** have been reported so far, exclusively with structurally rigid olefinic or aromatic halogen bond donors containing bromine or iodine atoms. So far, no study has addressed formation of **acr** or **phen** cocrystals with aliphatic, structurally flexible halogen-bond donors. At the same time, formation of halogen-bonded cocrystals was explored by the Aakeröy group as a means to obtain thermally stable materials involving volatile components such as **ofib** and related halogen bond donors.[46]

We now describe the synthesis, from solution and by mechanochemistry,[47,48] crystal structures and bench stability of cocrystals (**acr**)$_2$(**ofib**), (**phen**)$_2$(**ofib**) and (**phen**)(**ofib**). While the herein described cocrystals are the first examples of acridine or phenazine combined with an aliphatic halogen bond donor, the extensive evaluation of their bench stability also provides further insight into halogen bond-driven cocrystallization as a route to stabilize volatile compounds in the solid state.[46,49] Importantly, whereas crystal engineering by cocrystal formation is often focused on structural analysis and development of increasingly efficient designs and routes for cocrystal synthesis, factors determining the overall stability of cocrystals still remain poorly understood.

This is surprising, as understanding and manipulating cocrystal stability is central to development of pharmaceutically-relevant materials with improved solubility, and in the design of materials for capture of volatile compound. The first systematic investigation of thermodynamic driving forces behind cocrystal formation was only recently reported by the Day group using periodic DFT calculations.[50] Consequently, we recognized the herein reported cocrystals as suitable models for a multi-faceted experimental and theoretical study of stability of cocrystals involving a volatile component, and in particular of the differences in stability of stoichiometric variations, *i.e.* cocrystals based on identical building blocks, but in different stoichiometric ratios.

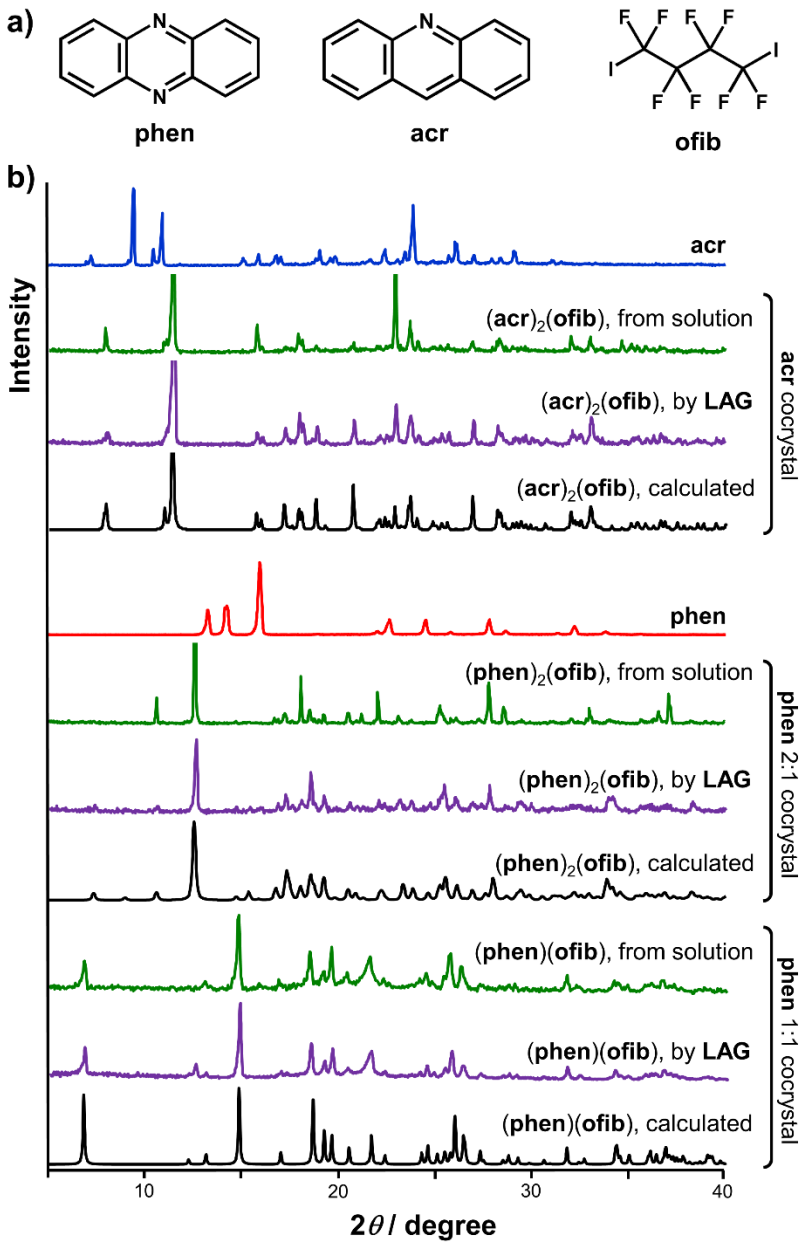

Figure 1. a) Molecular schemes of phenazine (**phen**), acridine (**acr**) and octafluoro-1,4-diiodobutane (**ofib**); b) comparison of relevant PXRD patterns for **ofib** cocrystals of **acr** and **phen** obtained from solution, by mechanochemistry, and simulated for the herein reported crystal structures.

Experimental

Phenazine was obtained from Merck. Acridine and octafluoro-1,4-diiodobutane were obtained from Sigma-Aldrich. Acetonitrile was purchased from J. T. Baker. Nitromethane was purchased from Fluka.

Solution syntheses. Single crystals of (**phen**)$_2$(**ofib**) suitable for X-ray diffraction were obtained by dissolving a mixture of **phen** (30 mg, 0.17 mmol) and **ofib** (60 μL, 0.33 mmol) in 1.5 mL of hot nitromethane, and the subsequent cooling and solvent evaporation at room temperature. Single crystals of (**phen**)(**ofib**) were obtained by dissolving a mixture of **phen** (45 mg, 0.25 mmol) and **ofib** (50 μL, 0.27 mmol) in 0.25 mL of hot chloroform, and the subsequent cooling and solvent evaporation at room temperature. Single crystals of (**acr**)$_2$(**ofib**) were obtained by dissolving a mixture of **acr** (30 mg, 0.17 mmol) and **ofib** (20 μL, 0.11 mmol) in 2 mL of hot acetonitrile, and the subsequent cooling and solvent evaporation at room temperature.

Mechanochemical syntheses. Milling was conducted in a Retsch MM200 mill operating at 25 Hz frequency using either a 10 mL SmartSnap stainless steel jar (Form-Tech Scientific, Inc.) equipped with two stainless-steel balls 7 mm in diameter (1.3 grams weight for each ball), or a 14 mL polytetrafluoroethylene (PTFE) jar equipped with one zirconia ball of 10 mm diameter (4 grams weight). All syntheses were repeated to ensure reproducibility and performed under the usual laboratory conditions (temperature ca. 25 °C, 40–60% relative humidity).

Synthesis of (**phen**)$_2$(**ofib**). In a representative synthesis, a mixture of **phen** (71 mg, 0.39 mmol) and **ofib** (37 μL, 0.20 mmol) was placed in a stainless steel jar along with 15 μL of nitromethane, and two stainless steel balls. The mixture was then milled for 15 minutes.

Synthesis of (**phen**)(**ofib**). In a representative synthesis, **phen** (45 mg, 0.25 mmol) and **ofib** (50 μL, 0.27 mmol, slight excess to compensate for evaporative loss of volatile **ofib** during synthesis) were placed in a PTFE jar along with 20 μL of nitromethane and a zirconia ball. The mixture was

then milled for 15 minutes. The cocrystal can also be obtained under different conditions, for example by milling neat reactants without any liquid added.

Synthesis of (**acr**)$_2$(**ofib**). A mixture of **acr** (71 mg, 0.40 mmol) and **ofib** (37 μL, 0.20 mmol) was placed in a stainless steel jar, along with 15 μL of acetonitrile and two stainless steel balls, and milled for 15 minutes.

Thermal analysis. Differential scanning calorimetry (DSC) measurements were performed on a Mettler-Toledo DSC823^e module in sealed aluminum pans (40 μL) with three pinholes in the lid, heated in a stream of nitrogen (150 mL min^{-1}) at a heating rate of 10 °C min^{-1}.

Thermogravimetric analysis (TGA) measurements were performed on a Mettler-Toledo TGA/SDTA 851e module in sealed aluminum pans (40 μL) with three pinholes in the lid, heated in a stream of nitrogen (150 mL min^{-1}) at a heating rate of 10 °C min^{-1}. Simultaneous TGA and DSC measurements were performed using a Mettler-Toledo TGA/DSC 1 thermal analyzer in open alumina crucibles (70 μL), heated in a stream of nitrogen (50 mL min^{-1}) up to 500 °C and a stream of air (50 mL min^{-1}) above 500 °C, at a heating rate of 10 °C min^{-1}. Data collection and analysis were performed using the STAR^e Software 14.00 and 15.00 program packages.[51]

Results of thermal analysis measurements are shown in Supplementary Information, figures S4-S6.

X-ray single crystal diffraction. Details of single crystal X-ray diffraction data collection and crystal structure refinement are listed in Table 1. The single crystal diffraction data for (**phen**)$_2$(**ofib**) were collected at 150 K and data for (**acr**)$_2$(**ofib**) at 295 K. Diffraction measurements were made on an Oxford Diffraction Xcalibur Kappa CCD X-ray diffractometer using graphite-monochromated Mo$K\alpha$ (λ = 0.71073Å) radiation. The data sets were collected using ω-scan mode

with 2θ up to 54°. Programs CrysAlis CCD and CrysAlis RED were employed for data collection, cell refinement, and data reduction.[52]

Single crystal X-ray diffraction data for (**phen**)(**ofib**) were collected both at 100K and 253K on a Bruker D8 Venture dual-source diffractometer equipped with a PHOTON II detector and an Oxford Cryostream 800 cooling system, using mirror-monochromatized Mo*K*α radiation (λ = 0.71073 Å) from a microfocus source, Data were collected in a series of φ- and ω-scans. APEX3 software was used for data collection, integration and reduction.[53] Semi-empirical (for datal collected at 100K) or numerical (data collected at 253K) absorption corrections were applied using SADABS-2016/2.[54] The structures were solved by direct or dual space iterative methods respectively using SHELXS[55] or SHELXT[56] and refined by full-matrix least-squares on F^2 using all data with SHELXL[57] within the OLEX2[58] and/or WinGX[59] environment. Hydrogen atoms were placed in calculated positions and treated as riding on the parent carbon atoms with U_{iso}(H) = 1.2 U_{eq}(C). Crystal structures figures were generated using MercuryCSD.[60] CCDC deposition numbers 1811939-1811942 contains crystallographic data for this paper. These data can be obtained free of charge *via* www.ccdc.cam.ac.uk/conts/retrieving.html or from the CCDC, 12 Union Road, Cambridge CB2 1EZ, UK.

Table 1. General and crystallographic information for herein reported cocrystals of **acr** and **phen**.

Cocrystal	(**acr**)$_2$(**ofib**)	(**phen**)$_2$(**ofib**)	(**phen**)(**ofib**) (100K)	(**phen**)(**ofib**) (253K)
CCDC Number	1811939	1811940	1811941	1811942
Formula	$C_{30}H_{18}F_8I_2N_2$	$C_{28}H_{16}F_8I_2N_4$	$C_{16}H_8F_8I_2N_2$	$C_{16}H_8F_8I_2N_2$
M_r	812.26	814.25	634.04	634.04
T (K)	295.0(1)	150.0(1)	100.0(1)	253.0(1)
Crystal system	monoclinic	triclinic	triclinic	triclinic
Space group	$P2_1/c$	$P\bar{1}$	$P\bar{1}$	$P\bar{1}$
a (Å)	11.1081(8)	5.7778(2)	4.9296(5)	4.9982(3)
b (Å)	5.8228(3)	9.9952(3)	7.6029(8)	7.6510(5)
c (Å)	22.5517(14)	12.1518(4)	13.2336(13)	13.2612(8)
α (°)	90	79.775(3)	79.905(3)	79.741(2)
β (°)	92.056(6)	86.343(3)	81.498(3)	81.6109(19)
γ (°)	90	82.478(3)	72.081(3)	72.9118(19)
V (Å^3)	1457.71(16)	684.09(4)	462.28(8)	474.62(5)

Z	2	1	1	1
ρ_{calc} (g cm^{-3})	1.85	1.98	2.28	2.22
μ (mm^{-1})	2.232	2.380	3.483	3.392
F(000)	780	390	296	296
Crystal size (mm^3)	0.35×0.22×0.10	0.67×0.43×0.22	0.25×0.20×0.05	0.894×0.471×0.127
θ range for data collection (°)	3.939-24.985	3.902-24.999	2.843-37.241	2.814-37.166
Reflections collected [R_{int}]	7739 [0.0280]	4762 [0.0143]	28188 [0.0359]	24980 [0.0457]
Reflections [$I > 2\sigma(I)$]	1925	2267	4296	3810
Data completeness (%)	99.1 to θ = 24.985°	99.0 to θ = 24.999°	99.6 to θ = 25.25°	98.2 to θ = 25.25°
Data/restraints/parameters	2538/0/190	2378/0/190	4517/0/128	4595/0/128
Goodness-of-fit on F^2	0.948	1.118	1.099	1.038
Final R for data with $I > 2\sigma(I)$	R_1 = 0.0355 wR_2 = 0.0826	R_1 = 0.0164 wR_2 = 0.0446	R_1 = 0.0173 wR_2 = 0.0372	R_1 = 0.0290 wR_2 = 0.0682
Final R for all data	R_1 = 0.0483 wR_2 = 0.0855	R_1 = 0.0177 wR_2 = 0.0450	R_1 = 0.0197 wR_2 = 0.0377	R_1 = 0.0403 wR_2 = 0.0727
Largest diff. peak/hole (e Å^{-3})	1.834/−0.536	0.429/−0.497	0.801/−0.586	0.923/−1.053

Powder X-Ray Diffraction. PXRD experiments were performed on a PHILIPS PW 1840 X-ray diffractometer with Cu$K\alpha_1$ (1.54056 Å) radiation source operating at 40 mA and 40 kV, equipped with a scintillation counter detector, in the 2θ range of 5-40°, step sizes in the range of 0.02 – 0.03° and measuring times of 0.2 – 0.5 seconds per step. In case of (**phen**)(**ofib**), PXRD experiments were performed on a Proto AXRD X-ray diffractometer, using a 600 W Cu$K\alpha$ (λ = 1.54184 Å) radiation source and a Dectris MYTHEN 1K one-dimensional linear detector, in the 2θ range of 4-40°, step size of 0.02° and a measuring time of 2 seconds per step. Data collection and analysis was performed using the program package Philips X'Pert.[61]

Real-time powder X-ray diffraction experiments and Rietveld analysis. For *in situ* stability studies,[62,63] experiments were performed on a Proto AXRD X-ray diffractometer, using a 600 W Cu$K\alpha$ (λ=1.54184 Å) radiation source and a Dectris MYTHEN 1K one-dimensional linear detector, in the 2θ range of 4-40°, step size of 0.02° and a measuring time of 2 seconds per step. The temperature inside the sample chamber was measured with a thermocouple sensor and was determined to be 25 °C ± 2 °C. Consecutive PXRD patterns were recorded in 7 minute intervals. Collected results were processed using an in-house designed MathLab script, and Rietveld[64]

quantitative phase analysis of real-time PXRD data was performed using the program TOPAS Academic 6. The series of PXRD scans were refined sequentially, refinable parameters included zero-point error, coefficients of Chebyshev polynomial to model background, peak shape parameters (pseudo-Voigt curve) and scale factors for the crystalline phases present in the reaction mixtures. The resulting weight fractions were converted into molar fractions which were used for plotting the kinetic curves.

Infrared spectroscopy. Fourier-transform infrared attenuated total reflectance (FTIR-ATR) measurements were performed on a Bruker VERTEX 70 instrument equipped with a single reflection diamond crystal PLATINUM ATR unit. Infrared spectra for all materials are shown in Supplementary Information, figures S7-S11.

Computational procedures. The energies of (**phen**)$_2$(**ofib**), (**phen**)(**ofib**), (**acr**)$_2$(**ofib**) as well as **phen** (α and β polymorphs) and **acr** (polymorphs III and VII) crystal structures were calculated with periodic DFT code CASTEP.[65] Crystal structures were geometry-optimized with respect to atom coordinates and unit cell dimensions, subject to the space group symmetry constraints. Calculations were performed using PBE functional and the van der Waals interactions were described with Grimme D2 dispersion correction.[66-69] The basis set of plane waves was truncated at 750 eV and norm-conserving OPIUM pseudopotentials[70] were used to simplify the Coulomb potential in the vicinity of atom nuclei. The Brillouin zone was sampled using a Monkhorst-Pack[71] k-point grid of 0.03 Å^{-1} spacing. The following convergence criteria were used: maximum energy change 10^{-5} eV/atom, maximum force on atom 0.03 eV/Å, maximum atom displacement 0.001 Å and residual stress 0.05 GPa.

In addition to the crystal structures we have approximated the gas-phase energy of **ofib** by placing an **ofib** molecule within a cubic cell and performing geometry optimization, whilst keeping the

cell dimensions fixed. The Gamma k-point was used to sample the Brillouin zone. Convergence with respect to unit cell size was performed and energies were calculated for cell edges of 20 Å, 25 Å and 30 Å length. It was found that 30x30x30 $Å^3$ is sufficiently large for the total energy to converge within 10^{-5} eV/atom.

Results and Discussion

Cocrystallization of **phen** and **acr** with **ofib** was explored through mechanochemical liquid-assisted grinding (LAG),[72-74] as well as by crystallization from solution. For both **acr** and **phen**, mechanochemical screening was conducted using 1:1 and 2:1 stoichiometric ratios of the halogen bond acceptor and **ofib**. In each case, milling yielded products with powder X-ray diffraction (PXRD) patterns different to those of starting materials. The PXRD patterns of milled products revealed the complete disappearance of Bragg reflections associated with **acr** of **phen** starting materials, indicating complete conversion of the halogen bond donor acceptors. In particular, PXRD analysis revealed that milling **acr** and **ofib** in either 1:1 or 2:1 respective stoichiometric ratio produces the same material, which was subsequently identified as a cocrystal of composition (**acr**)$_2$(**ofib**). In contrast, milling of **phen** and **ofib** in 1:1 and 2:1 stoichiometric ratios led to products with very different PXRD patterns, indicating the formation of cocrystals with compositions (**phen**)$_2$(**ofib**) and (**phen**)(**ofib**).

The formation of cocrystals (**acr**)$_2$(**ofib**), (**phen**)$_2$(**ofib**) and (**phen**)(**ofib**) was confirmed by screening for cocrystal formation from solution, which also produced diffraction-quality single crystals for each of the cocrystals, enabling crystal structure determination by X-ray crystallography (Table 1). Importantly, the PXRD patterns for solution-grown samples of

(**acr**)$_2$(**ofib**), (**phen**)$_2$(**ofib**) and (**phen**)(**ofib**) were in agreement with analogous samples prepared by mechanochemistry. Single crystal X-ray diffraction on a crystal of (**acr**)$_2$(**ofib**) grown from acetonitrile revealed the formation of three-component halogen-bonded assemblies in which a single molecule of **ofib** bridges two **acr** molecules *via* I···N halogen bonds of 3.044 (4) Å. This distance is 13.7 % less than the sum of the van der Waals radii of nitrogen (1.55 Å) and iodine (1.98 Å) (Figure 2a), corresponding to R_{XB} of 0.862.[75,76] The assemblies exhibited a pronounced step-like geometry, with two **acr** molecules in each assembly sitting in parallel planes separated by 4.71 Å (Figure 2b). Crystal structure analysis did not reveal any particularly short interactions between neighboring assemblies of (**acr**)$_2$(**ofib**), which assemble into a herringbone pattern *via* edge-to-face C-H· · · π contacts involving nearest-neighbor molecules of **acr**. Importantly, the three-dimensional arrangement of (**acr**)$_2$(**ofib**) assemblies leads to segregation of fluorinated and hydrocarbon components of the structure, typically observed in halogen-bonded cocrystals involving hydrocarbons and perfluorocarbons, as all **ofib** molecules stack to form columns parallel to the crystallographic *b*-axis.

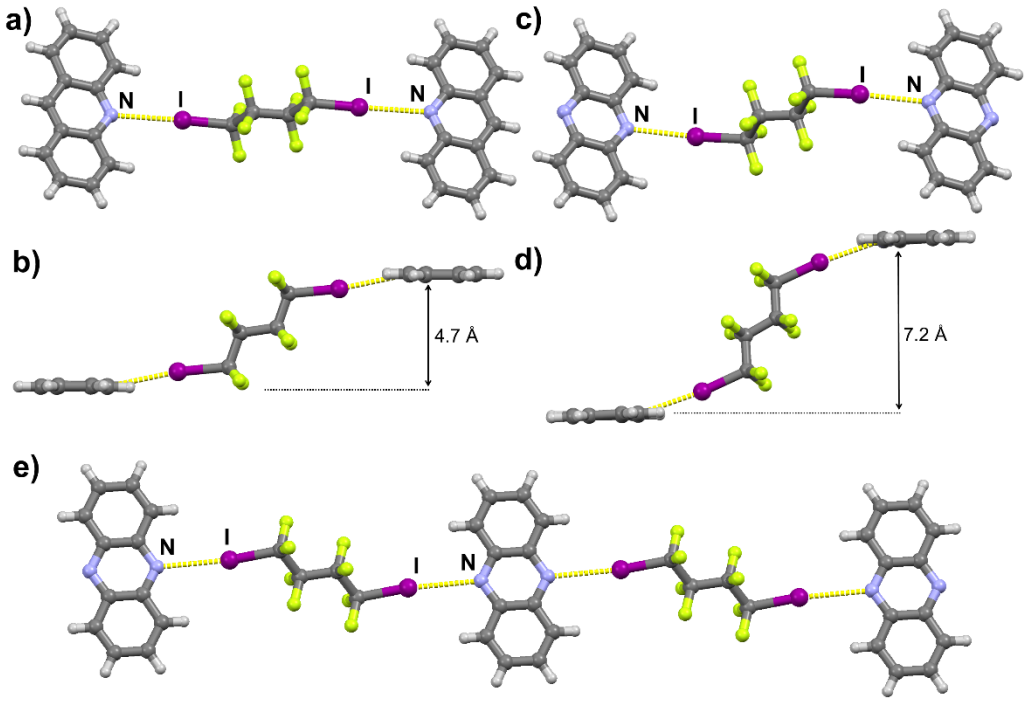

Figure 2. Crystal structures of cocrystals (**acr**)$_2$(**ofib**), (**phen**)$_2$(**ofib**) and (**phen**)(**ofib**). A single three-component halogen-bonded assembly in the cocrystal (**acr**)$_2$(**ofib**) viewed: (a) from the top and (b) from the side, illustrating the 4.7 Å step between the planes defined by **acr** molecules. A single three-component halogen-bonded assembly in the cocrystal (**phen**)$_2$(**ofib**) viewed: (c) from the top and (d) from the side, illustrating the 7.2 Å step between the planes defined by **phen** molecules. (e) Fragment of a supramolecular halogen-bonded chain in the structure of (**phen**)(**ofib**). Halogen bonds are shown as yellow dotted lines.

Crystal structure analysis of (**phen**)$_2$(**ofib**) reveals the formation of three-component halogen-bonded assemblies, resembling those in (**acr**)$_2$(**ofib**) (Figure 2c). The assemblies, held by I···N halogen bonds of 2.914(2) Å (17.5% shorter than the expected sum of van der Waals radii of iodine and nitrogen, R_{XB} of 0.825) adopt a step-like geometry in which the **phen** molecules form parallel planes separated by 7.21 Å (Figure 2d). The significantly larger size of the step defined by the halogen bond acceptors in the assemblies of (**phen**)$_2$(**ofib**), compared to those of

(**acr**)$_2$(**ofib**), is associated with a difference in orientation of the **ofib** halogen bond donor with respect to attached polycyclic halogen bond acceptors. In both cocrystals, the **ofib** molecule adopts a planar conformation with all -CF_2- groups adopting a staggered conformation, and sits in a plane that is almost perpendicular to the planes defined by the molecule of the halogen bond acceptor molecules: 86.7° for (**acr**)$_2$(**ofib**) and 77.0° for (**phen**)$_2$(**ofib**). However, in (**acr**)$_2$(**ofib**) the C-I bond of the halogen bond donor is almost parallel to the acceptor, forming an angle of 6° with the plane defined by the attached **acr** molecule. For (**phen**)$_2$(**ofib**), this angle is much larger, 26°, resulting in a more pronounced separation of the **phen** molecules in each assembly.

The most significant difference between the crystal structures of (**acr**)$_2$(**ofib**) and (**phen**)$_2$(**ofib**) arises from the formation of intermolecular C-H···N hydrogen bonds between neighboring assemblies of (**phen**)$_2$(**ofib**). In particular, **phen** molecules from nearest-neighbor assemblies connect through pairs of C-H···N bonds of 3.584(3) Å length, forming $R_2^2(8)$ supramolecular ring motifs. As a result, the structure of (**phen**)$_2$(**ofib**) may be best described as composed of one-dimensional chains held by alternating sets of I···N halogen bonds and C-H···N hydrogen-bonded ring motifs.

The composition and structure of (**phen**)$_2$(**ofib**) is consistent with almost all previously reported structures of halogen-bonded cocrystals of **phen**, which reveal only one nitrogen atom of the heterocycle participating in halogen bond formation, with the other involved in the formation of C-H···N hydrogen-bonded $R_2^2(8)$ dimers observed in (**phen**)$_2$(**ofib**). In principle, each molecule of **phen** could also act as a ditopic halogen bond acceptor, with both nitrogen atoms involved in halogen bonding. This is demonstrated in the crystal structure of (**phen**)(**ofib**), which is a stoichiometric variation[77,78] of (**phen**)$_2$(**ofib**), containing the two cocrystal components in a 1:1 stoichiometric ratio. The structure of (**phen**)(**ofib**) consists of supramolecular chains of

alternating **ofib** and **phen** molecules held together by I···N halogen bonds of 3.065(2) Å, which is 13.1% shorter compared to the sum of van der Waals radii (Figure 2e) and corresponds to R_{XB} of 0.868. The mutual orientation of **ofib** and **phen** molecules in each chain of (**phen**)(**ofib**) is significantly different than seen in the assemblies of (**phen**)$_2$(**ofib**), as the long axis of **ofib** molecules is now aligned with the direction of chain propagation, resulting in an almost coplanar parallel alignment of halogen bond acceptor molecules, demonstrated by a separation of less than 0.25 Å between the planes defined by nearest-neighbor **phen** molecules in a chain. The neighboring halogen-bonded chains in (**phen**)(**ofib**) stack in parallel, resulting in a layered structure consisting of segregated aromatic hydrocarbon and aliphatic perfluorocarbon molecules. Based on our CSD survey, the structure of (**phen**)(**ofib**) is the second so far reported halogen-bonded cocrystal in which the **phen** molecule employs both nitrogen atoms for halogen bond formation.

The bench stability of all prepared cocrystals was evaluated by thermogravimetric analysis (TGA) and real-time observation of the materials by PXRD over several hours. Specifically, TGA demonstrated that a sample of (**acr**)$_2$(**ofib**) loses weight in two distinct steps (Figure S4). The first step takes place between ca. 100 °C and 150 °C and amounts to a loss of 57.6% of original sample weight, consistent with the 55.9% mass loss calculated for complete removal of **ofib** from (**acr**)$_2$(**ofib**). The second step of 42.3% of the initial sample weight takes place in the range of ca. 220 °C to 280 °C and is interpreted as complete loss of **acr** by evaporation. Consequently. thermal decomposition of (**acr**)$_2$(**ofib**) proceeds in a single step, described by Equation 1:

(**acr**)$_2$(**ofib**)(s) $\rightarrow$ 2 **acr**(s) + **ofib**(g) (Equation 1)

The differential thermal analysis (DTA) for (**acr**)$_2$(**ofib**) reveals that the first weight loss step coincides with two overlapping endothermic events, potentially indicating cocrystal melting taking place along with decomposition (Figure S4).

Similar behavior is also observed for (**phen**)$_2$(**ofib**), for which TGA also reveals two decomposition steps (Figure S5). However, the first step now takes place at a lower temperature (below 100 °C) and corresponds to the loss of 50.3% of the initial sample weight, which is reasonably close to the calculated **ofib** content of 55.8%. The second step, which takes place between ca. 150 °C and 250 °C, again leads to complete loss of sample weight, which is consistent with evaporative loss of residual **phen**. While differential scanning calorimetry (DSC, Figure S5) shows that each weight loss step in TGA thermogram of (**phen**)$_2$(**ofib**) is associated with broad endothermic events, an additional sharp endothermic signal at ca. 178 °C is consistent with melting of **phen** formed after **ofib** loss. Therefore, thermal decomposition of (**phen**)$_2$(**ofib**) proceeds *via* the Equation 2:

(**phen**)$_2$(**ofib**)(s) → 2 **phen**(s) + **ofib**(g) (Equation 2)

Combined TGA and DSC analysis of (**phen**)(**ofib**) reveals that the complete loss of **ofib**, as indicated by the reduction of sample weight by 70.8% (which compares well to 71.6% calculated for **ofib** content in the (**phen**)(**ofib**) composition), takes place through two closely spaced steps below 100 °C (Figure S6). The steps, which are difficult to resolve using TGA but are more clearly distinguished in the DSC thermogram, could tentatively be associated with a two-step process involving loss of **ofib**, first to form (**phen**)$_2$(**ofib**):

2 (**phen**)(**ofib**)(s) → (**phen**)$_2$(**ofib**)(s) + **ofib**(g) (Equation 3)

followed by further loss of **ofib** from (**phen**)$_2$(**ofib**) to form solid **phen**, according to Equation 2.

The DSC thermogram also reveals a sharp endothermic event at around 178 °C, which is consistent with melting of the residual solid **phen**. This signal overlaps with a broader endothermic event that is interpreted as complete evaporation of residual **phen** between ca. 150 °C and 250 °C.

Real-time PXRD monitoring of cocrystal dissociation

Differences in stability of the prepared cocrystals were also examined by real-time PXRD monitoring of the three materials upon standing in open air. Direct observation of a sample of (**acr**)$_2$(**ofib**) revealed slow decomposition leading to the concomitant formation of acridine polymorphs III (CCDC code ACRDIN07) and VII (CCDC code ACRDIN06), consistent with the process that was described by Equation 1 (Figure 3a). Rietveld analysis of the PXRD data revealed that the material after ca. 2.5 hours still contains a substantial amount (~50 mol%) of (**acr**)$_2$(**ofib**) (Figure 3b). In contrast, the cocrystal (**phen**)$_2$(**ofib**) decomposed into α-phenazine (CCDC code PHENAZ04) and traces of its β-polymorph (CCDC code PHENAZ11), following the reaction of Equation 2, much more rapidly: decomposition to reach a similar content of residual (**phen**)$_2$(**ofib**) took place within ~30 minutes, and cocrystal phase has completely disappeared within ~3.5 hours (Figures 3c,d). The cocrystal (**phen**)(**ofib**) exhibited the poorest stability of all herein investigated phases (Figure 3e). During sample preparation, it already partially decomposed into solid α-phenazine, as indicated by Rietveld analysis of the first collected PXRD pattern, and the content of cocrystal phase fell below 50 mol% within ~10 minutes (Figure 3f). The cocrystal phase has almost completely disappeared within 90 minutes. Real-time monitoring reveals that the degradation of (**phen**)(**ofib**) simultaneously generates solid

phenazine and solid (**phen**)$_2$(**ofib**), indicating that partial decomposition described by reaction Equation 3, proceeds in parallel with a direct decomposition pathway described by the Equation 4:

(**phen**)(**ofib**) (s) → **phen** (s) + **ofib**(g) (Equation 4)

The final product of decomposition is solid α-phenazine, indicating that any (**phen**)$_2$(**ofib**) formed also decomposes, following the process of Equation 2. Indeed, the time-resolved PXRD measurements reveal that the rate of formation of solid phenazine slows down in the period between ca. 80 and 180 minutes since the beginning of the measurement (Figure 3f). After this, the rate of solid phenazine formation again increases, leading to complete conversion. The reduction in the rate of formation of **phen** coincides well with the appearance of (**phen**)$_2$(**ofib**), indicating that it is related to complete disappearance of more reactive (**phen**)(**ofib**) by pathways described by Equations 3 and 4. The subsequent increase in the rate of formation of phenazine is coincident with disappearance of (**phen**)$_2$(**ofib**), indicating it is associated with the degradation of that cocrystal phase following Equation 2.

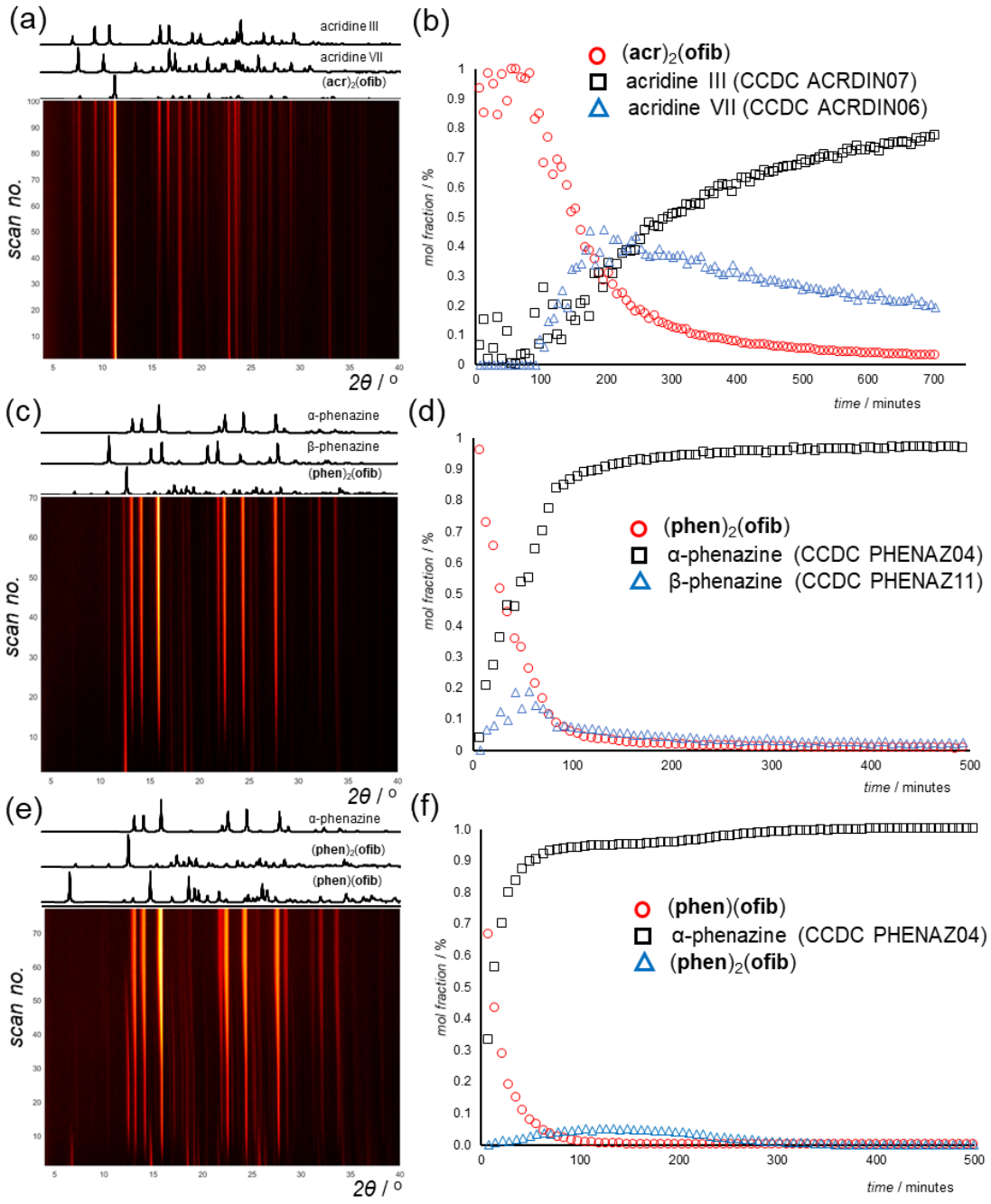

Figure 3. Results of real-time PXRD monitoring[62] of the decomposition of cocrystals (**acr**)$_2$(**ofib**), (**phen**)$_2$(**ofib**) and (**phen**)(**ofib**) upon standing in air. (a) Time-resolved diffractogram for (**acr**)$_2$(**ofib**) and (b) corresponding time-dependent change in mol fraction of crystalline phases during cocrystal degradation, as established by Rietveld refinement. (c) Time-resolved

diffractogram for (**phen**)$_2$(**ofib**) and (d) corresponding time-dependent change in mol fraction of crystalline phases during cocrystal degradation, as established by Rietveld refinement. (e) Time-resolved diffractogram for (**phen**)(**ofib**) and (f) corresponding time-dependent change in mol fraction of crystalline phases during cocrystal degradation, as established by Rietveld refinement. The time difference between consecutive scans in images (a), (c) and (e) is 7 minutes.

The cocrystals of **acr** and **phen** exhibit significant differences in stability, with the stability of the (**phen**)(**ofib**) cocrystal, in which each of the **phen** molecules is held by two halogen bonds, being particularly low. Consequently, we attempted to explore the enthalpic stability of the prepared phases through dispersion-corrected periodic density functional theory (DFT) calculations, performed using CASTEP,[32,65,50,79-81] by evaluating the enthalpy changes associated with chemical reactions of Equations 1-4. The calculated enthalpies for the transformations of **phen** and **acr** cocrystals are summarized in Table 2.

Table 2. Calculated reaction enthalpies ($\Delta H°_{calc}$) for the decomposition reactions of **acr** and **phen** cocrystals.

Equation	Reaction	Product polymorph	$\Delta H°_{calc}$/kJ mol^{-1}
1	(**acr**)$_2$(**ofib**)(s) → 2 **acr**(s) + **ofib**(g)	**acr** III (CCDC ACRDIN07) **acr** VII (CCDC ACRDIN06)	105.15 105.31
2	(**phen**)$_2$(**ofib**)(s) → 2 **phen**(s) + **ofib**(g)	**phen** α (CCDC PHENAZ04) **phen** β (CCDC PHENAZ11)	99.15 101.70
3	2 (**phen**)(**ofib**)(s) → (**phen**)$_2$(**ofib**)(s) + **ofib**(g)	-	87.25
4	(**phen**)(**ofib**)(s) → **phen**(s) + **ofib**(g)	**phen** α (CCDC PHENAZ04) **phen** β (CCDC PHENAZ11)	93.20 94.47

The enthalpy for the decomposition of (**acr**)$_2$(**ofib**) described by Equation 1 was calculated as +105.15 kJ mol^{-1} for the formation of **acr** polymorph III, and as +105.31 kJ mol^{-1} for the formation of of polymorph VII of **acr**. The similarity of these two evaluations provides a

tentative explanation for the concomitant appearance of **acr** forms III and VII during cocrystal decomposition. The process of Equation 2, which corresponds to the complete degradation of (**phen**)$_2$(**ofib**) into α-phenazine and gaseous **ofib**, is calculated to be less endothermic, calculated at +99.16 kJ mol^{-1}. The DFT calculations reveal that the process of Equation 3, in which (**phen**)(**ofib**) undergoes partial decomposition into solid (**phen**)$_2$(**ofib**) and one equivalent of **ofib** gas, should be endothermic by +87.25 kJ mol^{-1}. Finally, the process of Equation 4, which represents the direct, complete dissociation of (**phen**)(**ofib**) into solid α-phenazine and one equivalent of **ofib** gas, is calculated to be endothermic by +93.20 kJ mol^{-1}. An analogous reaction to produce solid β-phenazine has a calculated enthalpy of +94.47 kJ mol^{-1}, indicating that thermodynamically more stable polymorph is the dominant product of the decomposition. Overall, the decomposition reaction of the **acr** cocrystal is calculated to be more endothermic than those of (**phen**)$_2$(**ofib**) and (**phen**)(**ofib**), which is indeed consistent with the slower rate of decomposition of (**acr**)$_2$(**ofib**) compared to the two phenazine cocrystals. Specifically, the calculated ordering of the stabilities of cocrystals towards decomposition into solid **acr** or **phen** is (**acr**)$_2$(**ofib**) > (**phen**)$_2$(**ofib**) > (**phen**)(**ofib**), which is in qualitative agreement with the observed stability of the cocrystals in air. This sequence of stability is also in qualitative agreement with the decreasing basicity of halogen bond acceptor, which can be estimated by differences in pK_a values for acridine (pK_a=5.58), phenazine (pK_a=1.21) and protonated phenazine (pK_a=-4.30).[82] However, the accuracy of the absolute enthalpies obtained from DFT calculations cannot yet be evaluated in the absence of dedicated calorimetric measurements. In that context, it is important to note that the endothermic nature of reactions described by Equations 2 and 4, *i.e.* direct decomposition of (**phen**)$_2$(**ofib**) and (**phen**)(**ofib**) cocrystals into solid phenazine and **ofib** gas, is also evident from thermal analysis. The enthalpy of **ofib** loss can be estimated by

integrating the first endothermic event in the DSC thermogram of (**phen**)$_2$(**ofib**), leading to a value of +60.3 kJ mol^{-1}. Similarly, integration of the first two closely spaced endothermic events for (**phen**)(**ofib**) gives a value of +61.7 kJ mol^{-1} for complete loss of **ofib**. While such a calculation is not possible for (**acr**)$_2$(**ofib**), as cocrystal decomposition might be overlapping with cocrystal melting, the decomposition for this cocrystal takes place at a higher temperature, further confirming its higher stability compared to cocrystals of **phen**.

As all three observed pathways for the degradation of phenazine cocrystals are expected to be highly endothermic, we believe that these reactions are most likely driven by the entropic effect of losing a gaseous component. While DFT calculations of reaction enthalpies indicate that the (**phen**)(**ofib**) cocrystal should be less stable than its stoichiometric variation (**phen**)$_2$(**ofib**), the difference in stabilities might be additionally exacerbated by differences in crystal structures. Specifically, the analysis of the crystal structure of (**phen**)(**ofib**) reveals a layered structure in which the loss of **ofib** molecules could tentatively happen along a number of directions in the *ab*-crystallographic plane (Figures 4a,b). In contrast, the crystal structure of (**phen**)$_2$(**ofib**) consists of columns of **ofib** molecules that are parallel to the crystallographic *a*-axis and are completely surrounded by **phen** molecules, providing significantly less opportunity for **ofib** loss and cocrystal degradation (Figure 4c).

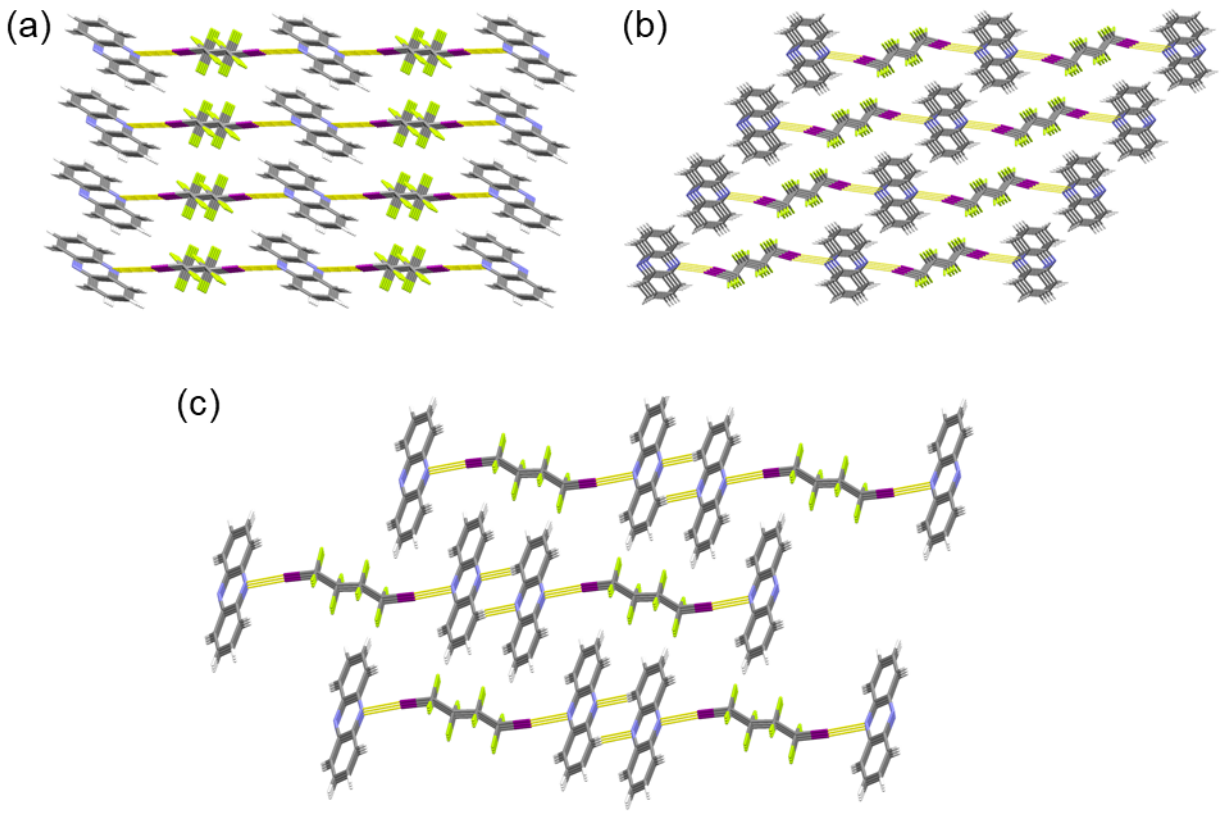

Figure 4. Views of the crystal structures of cocrystals of (**phen**)(**ofib**) and (**phen**)$_2$(**ofib**). The structure of (**phen**)(**ofib**) as seen along the: (a) *b*- and (b) *a*-crystallographic direction, providing different views of molecular layers parallel to the *ab*-crystallographic plane. (c) Structure of (**phen**)$_2$(**ofib**) viewed parallel to the crystallographic *a*-direction, illustrating columns of **ofib** molecules completely surrounded by molecules of **phen**. Intermolecular I···N halogen bonds and C-H···N bonds are shown as dotted yellow lines.

Conclusion

In summary, we have explored the ability of polycyclic aromatic hydrocarbons acridine and phenazine to act as halogen bond acceptors for the formation of cocrystals with a volatile aliphatic halogen bond donor octafluoro-1,4- diiodobutane. Whereas both acridine and phenazine formed cocrystals containing the halogen bond acceptor and donor in a 2:1 stoichiometric ratio, the availability of an additional sp^2-hybridized nitrogen atom in phenazine enables the formation of a cocrystal stoichiometric variation containing the two components in a 1:1 stoichiometric ratio. Evaluation of thermal stability and bench stability of the three cocrystals reveals that acridine produces the most stable cocrystal, followed by cocrystals of phenazine with 2:1 and 1:1 stoichiometric ratios of halogen bond acceptor to donor. The higher stability of the acridine cocrystal is consistent with its more basic nature, reflected in a higher pK_a compared to phenazine. The difference in stabilities of the two stoichiometric variations of the phenazine cocrystal is notable, with the 1:1 cocrystal composition exhibiting a very significantly low bench stability, rapidly losing the halogen bond donor in open air to concomitantly form solid phenazine and the more stable cocrystal of 2:1 acceptor:donor stoichiometry. Importantly, the ranking of cocrystals by their relative stability, as measured by real-time X-ray powder diffraction monitoring and thermal analysis, is readily reproduced by dispersion-corrected periodic DFT calculations. The herein observed difference in stability of stoichiometrically different cocrystals of phenazine is most likely a result of thermodynamic and kinetic crystal structure-related factors, and highlights the still poorly understood observation that changing the stoichiometric composition of a cocrystal can lead to materials with improved stability.[83-86] As theoretical and experimental studies of cocrystal stability remain very rare, especially in the context of halogen-bonded materials, we believe that the herein demonstrated qualitative

agreement between experimental and theoretical assessments of cocrystal stability is of particular importance for understanding and, ultimately, designing cocrystal solids with desired stability. With that in mind, we are currently using experimental and theoretical techniques to evaluate differences in stability of other halogen-bonded cocrystals and stoichiometric variations.

ASSOCIATED CONTENT

Supporting Information. The following files are available free of charge.

Experimental details, including ORTEP images of asymmetric units of (**acr**)$_2$(**ofib**), (**phen**)$_2$(**ofib**) and (**phen**)(**ofib**), TGA/DTA and TGA/DSC thermograms, and infrared attenuated total reflectance (IR-ATR) spectra. (PDF)

Crystal structures in CIF format. The crystallographic data has also been submitted to the Cambridge Crystallographic Data Center under deposition codes CCDC 1811939-1811942. This data can be obtained free of charge via www.ccdc.cam.ac.uk/data_request/cif, or by emailing data_request@ccdc.cam.ac.uk, or by contacting The Cambridge Crystallographic Data Centre, 12, Union Road, Cambridge CB2 1EZ, UK; fax: +44 1223 336033.

AUTHOR INFORMATION

Corresponding Authors

*Dominik Cinčić, Department of Chemistry, Faculty of Science, University of Zagreb, Horvatovac 102a, HR-10000 Zagreb, Croatia. E-mail: dominik@chem.pmf.hr

*Tomislav Friščić, Department of Chemistry, McGill University, 801 Sherbrooke St. W. H3A 0B8 Montreal, Canada. E-mail: tomislav.friscic@mcgill.ca

Author Contributions

The manuscript was written through contributions of all authors. All authors have given approval to the final version of the manuscript.

Funding Sources

Croatian Science Foundation (HRZZ-IP-2014-09-7367); National Science and Engineering Research Council (NSERC) Discovery Grant (RGPIN-2017-06467); NSERC E. W. R. Steacie Memorial Fellowship (SMFSU 507347-17); Banting Fellowship program; Cardiff University; Senior Birmingham Fellowship, University of Birmingham (AJM).

ACKNOWLEDGMENT

We acknowledge financial support of the Croatian Science Foundation (HRZZ-IP-2014-09-7367). National Science and Engineering Research Council (NSERC) Discovery Grant (RGPIN-2017-06467), NSERC E. W. R. Steacie Memorial Fellowship (SMFSU 507347-17), Banting Fellowship program (FT), Cardiff University, UK (PH), AJM acknowledges financial support from the University of Birmingham through a Senior Birmingham Fellowship. Computations were made on the supercomputer Guillimin from McGill University, managed by Calcul Québec and Compute Canada. The operation of this supercomputer is funded by the Canada Foundation for Innovation (CFI), the ministère de l'Économie, de la science et de l'innovation du Québec (MESI) and the Fonds de recherche du Québec - Nature et technologies (FRQ-NT).

REFERENCES

(1) Cavallo, G.; Metrangolo, P.; Milani, R.; Pilati, T.; Priimägi, A.; Resnati, G.; Terraneo, G. *Chem. Rev.* **2016**, *116*, 2478–2601.

(2) Politzer, P.; Murray, J. S.; Clark, T. *Phys. Chem. Chem. Phys.* **2010**, *12*, 7748–7757.

(3) Priimägi, A.; Cavallo, G.; Metrangolo, P.; Resnati, G. *Acc. Chem. Res.* **2013**, *46*, 2686–2695.

(4) Metrangolo, P.; Neukirch, H.; Pilati, T.; Resnati, G. *Acc. Chem. Res.* **2005**, *38*, 386–395.

(5) Saccone, M.; Cavallo, G.; Metrangolo, P.; Pace, A.; Pibiri, I.; Pilati, T.; Resnati G.; Terraneo, G. *CrystEngComm* **2013**, *15*, 3102–3105.

(6) Cinčić, D.; Friščić T.; Jones, W. *Chem.-Eur. J.* **2008**, *14*, 747–753.

(7) Stilinović, V.; Horvat, G.; Hrenar, T.; Nemec V.; Cinčić, D. *Chem. Eur. J.* **2017**, *22*, 5244–5257.

(8) Aakeröy, C. B.; Wijethunga, T. K.; Desper J.; Đaković, M. *Cryst. Growth Des.* **2016**, *16*, 2662–2670. Cinčić, D.; Nemec, V. *CrystEngComm.* **2016**, *18*, 7425–7429.

(9) Zbačnik, M.; Vitković, M.; Vulić, V.; Nogalo, I.; Cinčić, D. *Cryst. Growth Des.* **2016**, *16*, 6381–6389.

(10) Cinčić, D.; Friščić, T.; Jones, W. *CrystEngComm.* **2011**, *13*, 3224–3231.

(11) Sgarbossa, P.; Bertani, R.; Di Noto, V.; Piga, M.; Giffin, G. A.; Terraneo, G.; Pilati, T.; Metrangolo, P.; Resnati, G. *Cryst. Growth Des.* **2012**, *12*, 297–305.

(12) Aakeröy, C. B.; Desper, J.; Fasulo, M.; Hussain, I.; Levin, B.; Schultheiss, N. *CrystEngComm* **2008**, *10*, 1816–1821.

(13) Lapadula, G.; Judaš, N.; Friščić, T.; Jones, W. *Chem. Eur. J.* **2010**, *16*, 7400–7403.

(14) Merkens, C.; Pan, F.; Englert, U. *CrystEngComm.* **2013**, *15*, 8153–8158.

(15) Bushuyev, O. S.; Tan, D.; Barrett, C. J.; Friščić, T. *CrystEngComm.* **2015**, *17*, 73–80.

(16) Cinčić, D.; Friščić, T. *CrystEngComm*. **2014**, *16*, 10169–10172.

(17) Troff, R. W.; Mäkelä, T.; Topić, F.; Valkonen, A.; Raatikainen, K.; Rissanen, K. *Eur. J. Org. Chem*. **2013**, 1617–1637.

(18) Cinčić, D.; Friščić, T.; Jones W. *J. Am. Chem. Soc*. **2008**, *130*, 7524–7525.

(19) Beale, T. M.; Chudzinski, M. G.; Sarwar, M. G., Taylor, M. S. *Chem. Soc. Rev*. **2012**, *134*, 8260–8267.

(20) Erdélyi, M. *Chem. Soc. Rev*. **2012**, *41*, 3547–3557.

(21) Wang, C.; Danovich, D.; Mo, Y.; Shaik, S. *J. Chem. Theory Comput*. **2014**, *10*, 3726–3737.

(22) Pinter, B.; Nagels, N.; Herrebout, W. A.; De Proft, F. *Chem.–Eur. J*. **2013**, *19*, 519–530.

(23) Nagels, N.; Geboes, Y.; Pinter, B.; De Proft, F.; Herrebout, W. A. *Chem.–Eur. J*. **2014**, *20*, 8433–8443.

(24) Bushuyev, O. S.; Friščić, T.; Barrett, C. J. *Cryst. Growth Des*. **2016**, *16*, 541-545.

(25) Bushuyev, O. S.; Corkery, T. C.; Barrett, C. J.; Friščić, T. *Chem. Sci*. **2014**, *5*, 3158-3164.

(26) Cinčić, D.; Friščić T.; Jones, W. *New J. Chem*. **2008**, *32*, 1776–1781.

(27) Cinčić, D.; Friščić, T.; Jones, W. *Chem. Mater*. **2008**, *20*, 6623–6626.

(28) Nemec, V.; Lisac, K.; Stilinović, V.; Cinčić, D. *J. Mol. Struct*. **2017**, *1128*, 400–409.

(29) S. Biella, M. Cametti, T. Caronna, G. Cavallo, A. Forni, P. Metrangolo, T. Pilati, G. Resnati, G. Terraneo *Supramol. Chem*. **2011**, *23*, 256-262.

(30) Catalano, L.; Metrangolo, P.; Pilati, T.; Resnati, G.; Terraneo, G.; Ursini, M. *J. Fluor. Chem.* **2017**, *196*, 32-36.

(31) Aakeröy, C. B.; Welideniya, D.; Desper, J.; Moore, C. *CrystEngComm* **2014**, *16*, 10203-10209.

(32) Szell, P. M. J.; Gabriel, S. A.; Gill, R. D. D.; Wan, S. Y. H.; Gabidullin, B.; Bryce, D. L. *Acta Crystallogr. C*, **2017**, *73*, 157-167.

(33) D. Fox, P. Metrangolo, D. Pasini, T. Pilati, G. Resnati, G. Terraneo *CrystEngComm* **2008**, *10*, 1132-1136.

(34) Aakeröy, C. B.; Wijethunga, T. K.; Desper, J.; Moore, C. *J. Chem. Cryst.* **2015**, *45*, 267-276.

(35) Crihfield, A.; Hartwell, J.; Phelps, D.; Bailey Walsh, R.; Harris, J. L.; Payne, J. F.; Pennington, W. T.; Hanks, T. W. *Cryst. Growth Des.* **2003**, *3*, 313-320.

(36) Corradi, E.; Meille, S. V.; Messina, M. T.; Metrangolo, P.; Resnati, G. *Tetrahedron Lett.* **1999**, *40*, 7519-7523.

(37) Vioglio, P. C.; Catalano, L.; Vasyleva, V.; Nervi, C.; Chierotti, M. R.; Resnati, G.; Gobetto, R.; Metrangolo, P. *Chem. Eur. J.* **2016**, *22*, 16819-16828.

(38) Aakeröy, C. B.; Wijethunga, T. K.; Haj, M. A.; Deper, J.; Moore, C. *CrystEngComm* **2014**, *16*, 7218-7225.

(39) Babu, N. J.; Nangia, A. *Cryst. Growth Des.* **2006**, *6*, 1753-1756.

(40) Ravat, P.; SeethaLekshmi, S.; Nandy Biswas, S.; Nandy, P.; Varughese, S. *Cryst. Growth Des.* **2015**, *15*, 2389-2401.

(41) Braga, D.; Grepioni, F.; Maini, L.; Mazzeo, P. P.; Rubini, K. *Thermochim. Acta* **2010**, 507–508.

(42) Lide, D. R. (ed.) *CRC Handbook of Chemistry and Physics, 84th Edition* **2003**, CRC Press LLC.

(43) Batchelor, E.; Klinowski, J.; Jones, W. *J. Mat. Chem.* **2000**, *10*, 839-848.

(44) Nguyen, K. L.; Friščić, T.; Day, G. M.; Gladden, L. F.; Jones, W. *Nature Mater.* **2007**, *6*, 206-209.

(45) Allen, F. H. *Acta Cryst. B*, **2002**, 58, 380–388.

(46) Aakeröy, C. B.; Wijethunga, T. K.; Benton, J.; Desper, J. *Chem. Commun.* **2015**, *51*, 2425–2428.

(47) Weyna. D. R.; Shattock, T.; Vishweshwar, P.; Zaworotko, M. J. *Cryst. Growth Des.* **2009**, *9*, 1106-1123.

(48) Braga, D.; Maini, L.; Grepioni, F. Chem. Soc. Rev. 2013, 42, 7638-7648.

(49) Metrangolo, P.; Carcenac, Y.; Lahtinen, M.; Pilati, T.; Rissanen, K.; Vij, A.; Resnati, G. *Science* **2009**, *323*, 1461−1464.

(50) Taylor, C. R.; Day, G. M. *Cryst. Growth Des.* **2018**, *18*, 892-904.

(51) STAR^{e} Software 14.00/15.00, Mettler-Toledo GmbH, 2015.

(52) Oxford Diffraction, Oxford Diffraction Ltd., Xcalibur CCD system, CrysAlis CCD and CrysAlis RED software, Version 1.170, 2003.

(53) Bruker. APEX3. Bruker AXS Inc., Madison, Wisconsin, USA, 2012.

(54) Krause, L.; Herbst-Irmer, R.; Sheldrick, G. M.; Stalke, D. *J. Appl. Cryst.*, **2015**, *48*, 3–10.

(55) Sheldrick, G. M. *Acta Cryst. A*, **2008**, *64*, 112–122.

(56) Sheldrick, G. M. *Acta Cryst. C*, **2015**, *71*, 3–8.

(57) Sheldrick, G. M. *Acta Cryst. A*, **2015**, *71*, 3–8.

(58) Dolomanov, O. V.; Bourhis, L. J.; Gildea, R. J.; Howard, J. A. K.; Puschmann, H. *J. Appl. Cryst.*, **2009**, *42*, 339–341.

(59) Farrugia, L. J. *J. Appl. Cryst.*, **2012**, *45*, 849–854.

(60) Macrae, C. F.; Bruno, I. J.; Chisholm, J. A.; Edgington, P. R.; McCabe, P.; Pidcock, E.; Rodriguez-Monge, L.; Taylor, R.; van de Streek, J.; Wood, P. A. *J. Appl. Crystallogr.* **2008**, *41*, 466.

(61) Philips X'Pert Data Collector 1.3e, Philips Analytical B. V. Netherlands, 2001; Philips X'Pert Graphic & Identify 1.3e Philips Analytical B. V. Netherlands, 2001; Philips X'Pert Plus 1.0, Philips Analytical B. V. Netherlands, 1999.

(62) Huskić, I.; Christopherson, J.-C.; Užarević, K.; Friščić, T. *Chem. Commun.* **2016**, *52*, 5120-5123.

(63) Užarević, K.; Wang, T. C.; Moon, S.-Y.; Fidelli, A. M.; Hupp, J. T.; Farha, O. K.; Friščić, T. *Chem. Commun.* **2016**, *52*, 2133-2136.

(64) Rietveld, H. M. *J. Appl. Crystallogr.* **1969**, *2*, 65.

(65) Clark, S. J.; Segall, M. D.; Pickard, C. J.; Hasnip, P. J.; Probert, M. I. J.; Refson, K.; Payne, M. C. *Z. Kristallogr.* **2005**, *220*, 567.

(66) Grimme, S. *J. Comput. Chem.* **2006**, *27*, 1787.

(67) The use of dispersion correction in modelling halogen bonding interactions is a very active area of research, see for example references 66 and 67.

(68) Anderson, L. N.; Aquino, F. W.; Raeber, A. E.; Chen, X.; Wong, B. M. *J. Chem. Theory Comput.* **2017**, DOI: 10.1021/acs.jctc.7b01078

(69) Kozuch, S.; Martin, J. M. L. *J. Chem. Theory Comput.* **2013**, *9*, 1918-1931.

(70) Ramer, N. J.; Rappe, A. M. *Phys. Rev. B* **1999**, *59*, 12471.

(71) Monkhorst, H. J.; Pack, J. D. *Phys. Rev. B* **1976**, *13*, 5188.

(72) Friščić, T.; Jones. W. *Cryst. Growth Des.* **2009**, *9*, 1621-1637.

(73) Do, J.-L.; Friščić, T. *Synlett* **2017**, *28*, 2066-2092.

(74) Friščić, T.; Trask, A. V.; Jones, W.; Motherwell, W. D. S. *Angew. Chem. Int. Ed.* **2006**, *45*, 7546-7550.

(75) Mantina, M.; Chamberlin, A. C.; Valero, R.; Cramer, C. J.; Truhlar, D. G. *J. Phys. Chem. A* **2009**, *113*, 5806-5812.

(76) Bondi, A. *J. Phys. Chem.* **1964**, *68*, 441-451.

(77) Trask, A. V.; van de Streek. J.; Motherwell, W. D. S.; Jones, W. *Cryst. Growth Des.* **2005**, *5*, 2233-2241.

(78) Karki, S.; Friščić, T.; Jones, W. *CrystEngComm* **2009**, *11*, 470-481.

(79) Xu, Y.; Viger-Gravel, J.; Korobkov, I.; Bryce, D. L. *J. Phys. Chem. C*, **2015**, *119*, 27104-27117.

(80) Szell, P. M. J.; Bryce, D. L. *J. Phys. Chem. C* **2016**, *120*, 11121-11130.

(81) Arhangelskis, M.; Eddleston, M. D.; Reid, D. G.; Day, G. M.; Bučar, D.-K.; Morris, A. J.; Jones, W. *Chem. Eur. J.* **2016**, *22*, 10065-10073.

(82) Grabowska, A.; Pakuła, B. *Photochem. Photobiol.* **1969**, *9*, 339-350.

(83) Matzger, A. J.; Li, Z. *Mol. Pharm.* **2016**, *13*, 990-995.

(84) Sarma, B.; Reddy, L. S.; Nangia, A. *Cryst. Growth Des.* **2008**, *8*, 4546-4552.

(85) Alhalaweh, A.; George, S.; Boström, D.; Velaga, S. P. *Cryst. Growth Des.* **2010**, *10*, 4847-4855.

(86) Alsirawan, MHD. B.; Vangala, V. R.; Kendrick, J.; Leusen, F. J. J.; Paradkar, A. *Cryst. Growth Des.* **2016**, *16*, 3072-3075.

For Table of Contents Use Only

Experimental and theoretical investigation of structures, stoichiometric diversity and bench stability of cocrystals with a volatile halogen bond donor

Katarina Lisac, Vinko Nemec, Filip Topić, Mihails Arhangelskis, Poppy Hindle, Ricky Tran, Igor Huskić, Andrew J. Morris, Tomislav Friščić and Dominik Cinčić**

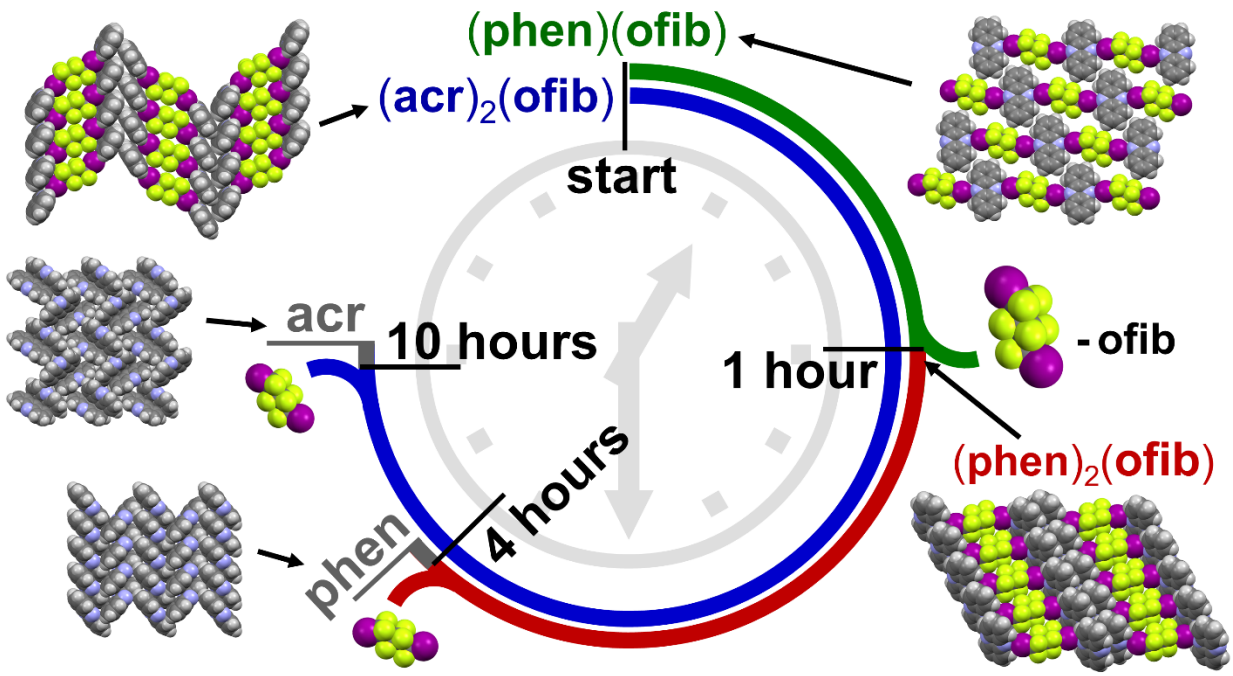

The structures, bench and thermal stability of halogen-bonded cocrystals of acridine and phenazine were explored using thermal analysis, real-time X-ray diffraction and theoretical calculations, revealing significant differences between cocrystals with different components and different stoichiometric compositions.